Deep Reasoning Networks for Unsupervised Pattern De-mixing with Constraint Reasoning

Di Chen [1] **Yiwei Bai** [1] **Wenting Zhao** [1] **Sebastian Ament** [1] **John M. Gregoire** [2] **Carla P. Gomes** [1]

Abstract

We introduce Deep Reasoning Networks (DRNets), an end-to-end framework that combines deep learning with constraint reasoning for solving pattern de-mixing problems, typically in an unsupervised or very-weakly-supervised setting. DRNets exploit problem structure and prior knowledge by tightly combining constraint reasoning with stochastic-gradient-based neural network optimization. Our motivating task is from materials discovery and concerns inferring crystal structures of materials from X-ray diffraction data (Crystal-Structure-Phase-Mapping). Given the complexity of its underlying scientific domain, we start by introducing DRNets on an analogous but much simpler task: de-mixing overlapping handwritten Sudokus (Multi-MNIST-Sudoku). On Multi-MNIST-Sudoku, DRNets almost perfectly recovered the mixed Sudokus' digits, with 100% digit accuracy, outperforming the supervised state-of-the-art MNIST de-mixing models. On Crystal-Structure-Phase-Mapping, DRNets significantly outperform the state of the art and experts' capabilities, recovering more precise and physically meaningful crystal structures.

1. Introduction

Deep learning has achieved tremendous success in areas such as vision, speech recognition, language translation, and autonomous driving. Nevertheless, certain limitations of deep learning are generally recognized, in particular, limitations due to the fact that deep learning approaches heavily depend on the availability of large amounts of labeled data. In certain domains, such as scientific discovery, it is often the case that scientists do not have large amounts of labeled data and instead have to rely on prior knowledge to make sense of the data. One grand challenge in scientific discovery is to perform high-throughput unsupervised interpretation of scientific data, given its exponential growth in generation rates, dramatically outpacing humans' ability to analyze them. Herein we consider pattern de-mixing problems, which involve decomposing a mixed signal into the collection of source patterns, such as separating mixtures of X-ray diffraction (XRD) signals into the source XRD signals of the corresponding crystal structures, a key challenge in materials discovery (Stanev et al., 2018; Gomes et al., 2019). More generally, pattern de-mixing problems are pervasive in scientific areas as diverse as biology, astronomy, and materials science, as well as in commercial applications, e.g., healthcare and music.

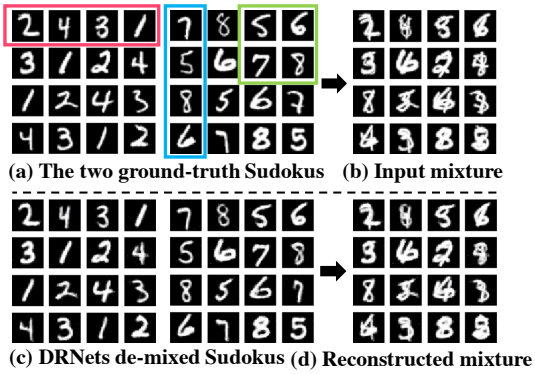

Figure 1. **(a)** Two 4x4 Sudokus: The cells in each row, column, and any of the four 2x2 boxes involving the corner cells have non-repeating digits. **(b)** Two overlapping Sudokus, with a mixture of two digits in each cell: one from 1 to 4 and the other from 5 to 8. **(c)** In **Multi-MNIST-Sudoku**, the digits of two overlapping hand written Sudokus (b) are de-mixed by DRNets. **(d)** DRNets' reconstructed overlapping hand written Sudokus.

We propose **Deep Reasoning Networks (DRNets)**, an end-to-end framework that combines deep learning with constraint reasoning for solving unsupervised or very-weakly-supervised pattern de-mixing tasks. DRNets are greatly motivated by a complex scientific discovery task that concerns inferring crystal structures of materials from X-ray diffraction data (Crystal-Structure-Phase-Mapping). Given the scientific complexity of this domain, we start by intro-

[1]Department of Computer Science, Cornell University, Ithaca, New York, USA [2]California Institute of Technology, Pasadena, California, USA. Correspondence to: Di Chen <di@cs.cornell.edu>.

Proceedings of the 37^{th} International Conference on Machine Learning, Online, PMLR 119, 2020.

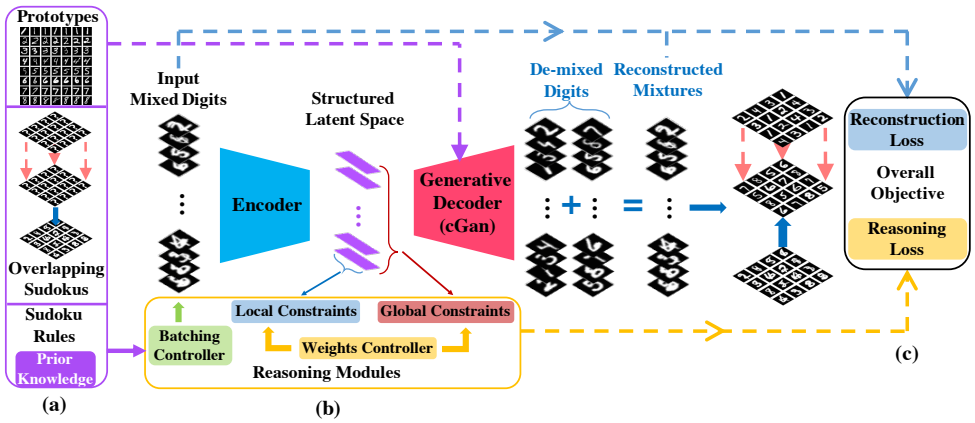

Figure 2. Deep Reasoning Networks (DRNets) perform end-to-end deep reasoning by encoding a latent space of the input data that is constrained to satisfy the Sudoku rules and is used by a generative decoder to generate the targeted output. **(a)** Prior knowledge includes prototypes of digits, which are used to pre-train and build the decoder's generative module, and the Sudoku rules, which help DRNets reason about the overlapping digits. **(b)** The reasoning modules batch data points involved in the same constraints (cells in rows, columns, blocks of a Sudoku) together, enforce that the latent space satisfies prior knowledge (Sudoku rules), and dynamically adjusts the weights of constraints based on their satisfiability. **(c)** The overall objective combines responses from the generative decoder, to reconstruct the input image, and responses from the reasoning modules, to enforce that the latent space adheres to the Sudoku constraints.

ducing DRNets on an analogous but much simpler task: disentangling two overlapping hand-written Sudokus (**Multi-MNIST-Sudoku**) (see Fig.1). Both de-mixing tasks require probabilistic reasoning to interpret noisy and uncertain data, while satisfying a set of rules: thermodynamic rules and Sudoku rules, respectively. For example, de-mixing hand written digits is challenging, but it is more feasible when we reason about the rules concerning the two overlapping Sudokus. Crystal structure phase mapping is yet substantially more complex. In fact, crystal structure phase mapping easily becomes too complex for experts to solve and is a major bottleneck in high-throughput materials discovery. Moreover, unlike the Multi-MNIST-Sudoku, where we can generate massive instances from MNIST dataset, scientific tasks such as crystal structure phase mapping often only have hundreds of data points and no labeled training data, which greatly challenges classical data-hungry deep learning models. Therefore, supervision by constraint reasoning is strongly desired, and strongly motivated by extensive prior knowledge from sources ranging from fundamental principles to the intuitive experience of scientists.

Our contributions: **(1)** We introduce an end-to-end framework named **Deep Reasoning Networks (DRNets)**, which combines deep learning with constraint reasoning for unsupervised or very-weakly-supervised de-mixing tasks. Specifically, DRNets perform end-to-end deep reasoning by encoding a latent space of the input data that captures the structure and prior knowledge constraints within and among data points (Fig.2). The latent space is used by a generative decoder to generate the targeted output, which should be consistent with the input data and prior knowledge. DRNets optimize an objective function capturing the overall problem objective as well as prior knowledge in the form of weighted constraints that control the encoding of the latent space. **(2)** We introduce a group of **entropy-based continuous relaxations** that use probabilistic modeling to encode general discrete constraints in DRNets, including sparsity, cardinality and so-called All-Different constraints. To optimize those constraints, we introduce constraint-aware stochastic gradient descent, which is a variant of standard SGD method (Robbins & Monro, 1985) that batches data points involved in the same constraint component together and dynamically adjust the constraints' weights as a function of their satisfiability. In the following sections, we show how to encode Multi-MNIST-Sudoku and Crystal-Structure-Phase-Mapping as DRNets, by properly defining the structure of the latent space, additional reasoning modules to model the problem constraints (prior knowledge), and the components of the objective function. De facto, these examples illustrate how to develop "gadgets" to encode a variety of constraints and prior knowledge in DRNets. **(3)** We demonstrate the potential of DRNets on two de-mixing tasks with detailed experimental results. We show how **(3.1)** DRNets significantly outperformed the state of the art and human experts on **Crystal-Structure-Phase-Mapping instances**, recovering more precise, interpretable, and physically meaningful crystal structure pattern decompositions. DRNets solved ***a previously unsolved chemical system***, which subsequently ***led to the discovery of a new material that is important for solar fuels technology.*** **(3.2)** On **Multi-MNIST-Sudoku instances**, without direct supervision, DRNets perfectly recovered the digits in the mixed Sudokus with 100% digit accuracy, outperforming the *supervised* state-of-the-art MNIST de-mixing models, including

CapsuleNet (Sabour et al., 2017) and ResNet (He et al., 2016).

2. Related Work

DRNets have been motivated by scientific tasks such as crystal phase mapping that involve identifying or de-mixing patterns in data that satisfy prior scientific knowledge. In general, for such tasks there are no labeled datasets. So our work focus on **unsupervised or very-weakly-supervised learning, using prior scientific knowledge.**

Most closely related work: Unsupervised or weakly supervised de-mixing approaches. Pattern de-mixing approaches have been developed under the name of *source separation* in the signal processing community. The unsupervised methods in this area mostly try to solve the de-mixing, which is in general ill-posed, using different regularizations. Among existing methods, recent work for weakly supervised audio source separation (Zhang et al., 2017) is most related to DRNets since they also utilize the information of pure source patterns to regularize/constrain the separated sources. However, their model learns a discriminator to discriminate the reality of separated sources, while DRNets utilize the generator of a pre-trained generative adversarial network (GAN) as the generative model of possible sources. Moreover, their model does not exploit any prior knowledge or constraint reasoning and therefore they need the true labels of mixed sources, which is almost the goal of our tasks, and therefore it is not applicable to our settings.

We now consider the state-of-the-art models for the tasks considered in this paper. For **Crystal-structure-phase-mapping**, due to the lack of labeled datasets, existing models (Ermon et al., 2015; Xue et al., 2017; Bai et al., 2017; 2018; Stanev et al., 2018) are mainly based on non-negative matrix factorization (NMF), which is in general unsupervised. Stanev et al. (2018) proposed the NMF-k algorithm, which applies a customized clustering process over the results of thousands of runs of pure NMF algorithm (Long et al., 2009) to cluster the common phase patterns. However, NMF-k does not enforce prior knowledge (namely thermodynamic rules) and therefore the solutions produced are often not completely physically meaningful. To address this limitation several approaches have been developed that use external mixed-integer programming modules to interact with the NMF de-mixing module to enforce prior knowledge (Ermon et al., 2015; Bai et al., 2017; 2018; Gomes et al., 2019). However, the coordination barrier between the NMF de-mixing module and the reasoning module often results in inferiror performance, where the solution satisfies constraints at the cost of huge reconstruction loss. In contrast to existing models, DRNets seamlessly integrate the pattern de-mixing module and the reasoning module, recovering almost exact ground truth decomposition. In our experiments we thoroughly compare DRNets' performance against the state of the art (IAFD (Gomes et al., 2019) and NMF-k (Stanev et al., 2018)) for crystal-structure pattern de-mixing. **MNIST de-mixing** was first studied by Hinton et al. in 2000, where the aim is to identify or de-mix overlapping digits coming from the MNIST datasets (LeCun et al., 1998). More recently, it has been tackled with state-of-the-art neural network models such as CapsuleNet (Sabour et al., 2017) and ResNet (He et al., 2016). Existing works concerning this task are mainly in supervised settings, where we have labels of digits for each overlapping image. However, in this paper, we aim to tackle this task in a very-weakly-supervised setting, where we only have access to the prototypes of single digits and the extra Sudoku rules. Due to the lack of existing models with the same setting, we compared DRNets' performance against the state-of-the-art supervised models (CapsuleNet and ResNet). By utilizing the supervision from prior knowledge and constraint reasoning, we show that DRNets' outperformed all supervised models with 100% digit accuracy.

Enhancing deep learning with symbolic prior knowledge. Exploiting problem structure and reasoning about prior knowledge has been of increasing interest to facilitate deep learning (Manhaeve et al., 2018; Garcez et al., 2019). In computer vision, symmetry constraints, bone-length constraints and linear constraints were introduced for human pose estimation (Zhou et al., 2017; 2016) and image segmentation (Pathak et al., 2015) to regularize the output and enhance generalization. In natural language processing, Hu et al. (2016a;b) introduced the *posterior regularization* (Ganchev et al., 2010) framework into deep learning to incorporate rule-based grammatical knowledge using first order logic. Xu et al. (2017) proposed a semantic loss function to enforce propositional logic constraints on the output of neural networks for semi-supervised multi-class classification tasks. Wang et al. (2019) proposed SATNet, which approximately encodes a MAXSAT solver into a neural network layer called SATNet layer, to explicitly learn the logical structures (e.g., parity function and Sudoku) from the labeled training data. Previous works in this area primarily focus on supervised or semi-supervised settings for data-rich domains, where direct supervision from labels reduce the importance of explicitly reasoning about prior knowledge. In contrast, with an unsupervised setting, the supervision of DRNets comes from reasoning about prior knowledge and self-reconstruction, which is strongly desired for problems in scientific discovery due to the lack of labeled datasets, and strongly motivated by extensive prior knowledge from sources ranging from fundamental principles to the intuitive experience of scientists. Among existing works, SATNet is mostly related to DRNets in the sense of bridging reasoning with deep learning. However, SATNet is essentially

designed for learning logical structures (prior knowledge) from labeled training examples while DRNets aim to facilitate unsupervised learning with known constraints. In terms of the encoding of the reasoning module, the semantic loss (Xu et al., 2017) is mostly related to ours. However, the semantic loss encodes constraints by propositional logic, which requires enumerating all possible Boolean assignments that satisfy the constraints. Consequently, the semantic loss has to enumerate a large number of assignments to encode constraints such as k-sparsity constraints and All-Different constraints, which is not applicable to tasks considered in this paper.

3. Deep Reasoning Networks

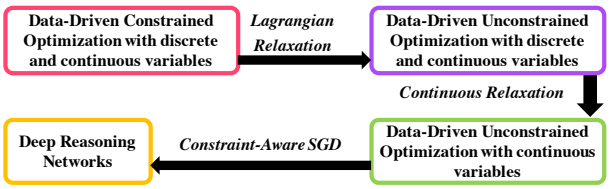

Figure 3. The reduction flow of Deep Reasoning Networks.

DRNets (see Fig. 2) are inspired by human reasoning (Shivhare & Kumar, 2016): we abstract patterns to higher-level descriptions and combine them with prior-knowledge to fill-in the gaps. Consider Multi-MNIST-Sudoku (Fig. 1): we first guess the digits in each cell based on the patterns; we re-adjust our initial beliefs and re-image the overlapping patterns by reasoning about Sudoku rules and comparing them to the original ones, potentially involving several iterations.

Formally, to leverage problem structure and prior knowledge using constraint reasoning, **DRNets formulate unsupervised pattern de-mixing as data-driven constrained optimization:**

$$\min_{\theta} \frac{1}{N}\sum_{i=1}^{N}\mathcal{L}(G(\phi_\theta(\mathbf{x}_i)),\mathbf{x}_i)$$
$$\text{s.t. } \phi_\theta(\mathbf{x}_i)\in\Omega^{\text{local}} \text{ and } (\phi_\theta(\mathbf{x}_1),...,\phi_\theta(\mathbf{x}_N))\in\Omega^{\text{global}} \quad (1)$$

In this formulation, N is the number of input data points, $\mathbf{x}_i \in R^n$ is the i-th n-dimensional input data point, $\phi_\theta(\cdot)$ is the function of the encoder in DRNets parameterized by θ, $G(\cdot)$ denotes the generative decoder, $\mathcal{L}(\cdot,\cdot)$ is the loss function (e.g., evaluating the reconstruction of patterns), Ω^{local} and Ω^{global} are the constrained spaces w.r.t. constraints involving a single input data point and constraints involving several input data points, respectively. $G(\cdot)$ is in general a fixed pre-trained or parametric generative model, which is obtained from either the prototypes or a theoretical model of pure patterns using prior knowledge. For example, in Multi-MNIST-Sudoku, $G(\cdot)$ is a pre-trained conditional GAN (Mirza & Osindero, 2014) using hand-written digits, and for Crystal-Structure-Phase-Mapping, $G(\cdot)$ is a Gaussian Mixture model based on *idealized* known pure crystal structures. Herein, the output of the encoder $\phi_\theta(\mathbf{x}_i)$ involves the encodings of the possible de-mixed pure patterns along with their probabilities. Furthermore, the encodings $\phi_\theta(\mathbf{x}_i)$ are constrained by space Ω^{local} and space Ω^{global} to satisfy prior knowledge. The generative decoder $G(\phi_\theta(\mathbf{x}_i))$ decodes $\phi_\theta(\mathbf{x}_i)$ into the potential corresponding pure patterns and remix them to reconstruct the input mixture $\mathbf{x}_i$.

Note that constraints can involve several (potentially all) data points: e.g., in Sudoku, all digits should form a valid Sudoku and in crystal-structure-phase-mapping, all data points in a composition graph should form a valid phase diagram. Thus, we specify local and global constraints in DRNets – local constraints only involve a single input data point whereas global constraints involve several input data points, and they are optimized using different strategies.

Solving the data-driven constrained optimization problem (1) directly is extremely challenging since the objective function in general involves deep neural networks, which are highly non-linear and non-convex, and prior knowledge often even involves combinatorial constraints (Fig.3). Therefore, we use Lagrangian relaxation to approximate equation (1) with an unconstrained optimization problem, i.e.,

$$\min_{\theta} \frac{1}{N}\sum_{i=1}^{N}\mathcal{L}(G(\phi_\theta(\mathbf{x}_i)),\mathbf{x}_i)+\lambda^l\psi^l(\phi_\theta(\mathbf{x}_i)) + \sum_{j=1}^{N_g}\lambda_j^g\psi_j^g(\{\phi_\theta(\mathbf{x}_k)|k\in S_j\}) \quad (2)$$

Here, N_g denotes the number of global constraints, S_j denotes the set of indices w.r.t. the data points involved in the j-th global constraint, and ψ^l, ψ_j^g denote the penalty functions for local constraints and global constraints, respectively, along with their corresponding penalty weights λ^l and λ_j^g. In the following, we propose two mechanisms to tackle the above unconstrained optimization task (Fig.3).

Continuous Relaxation: Prior knowledge often involves combinatorial constraints with discrete variables that are difficult to optimize in an end-to-end manner using gradient-based methods. Therefore, we need to design proper continuous relaxations for discrete constraints to make the overall objective function differentiable. Existing works (Hu et al., 2016a; Xu et al., 2017) proposed several relaxations for injecting first-order logic and propositional logic into deep learning. However, limited by the expressive power of those logic formulas, we would need a large number of logical terms to express constraints such as k-sparsity constraints or All-Different constraints. Therefore, to instantiate DRNets for our tasks, we propose a group of entropy-based continuous relaxations to encode general discrete constraints such as sparsity, cardinality and All-Different constraints (see Fig.4). We construct continuous relaxations based on probabilistic modelling of discrete variables, where we model a probability distribution over all possible values for each discrete variable. For example, in Multi-MNIST-Sudoku,

Cardinality Constraint	**Cardinality Constraint Relaxation**
$e_{i,j} \in \{0,1\}$ j = 1 ... 8 $s.t.\ \sum_{j=1}^{4} e_{i,j} = 1$ and $\sum_{j=5}^{8} e_{i,j} = 1$	$\min_{\theta} H(P_i) + H(Q_i) = -\sum_{j=1}^{4} P_{i,j} \log P_{i,j} - \sum_{j=1}^{4} Q_{i,j} \log Q_{i,j}$
All-Different Constraint	**All-Different Constraint Relaxation**
For all constrained set S $s.t. \sum_{i \in S} e_{i,j} = 1$ for j = 1 ... 8	For all constrained set S $\max_{\theta} H(\bar{P}_S) + H(\bar{Q}_S)$
k-Sparsity Constraint	**k-Sparsity Constraint Relaxation**
$e_{i,j} \in \{0,1\}$ j = 1 ... M $s.t. \sum_{j=1}^{M} e_{i,j} \leq k$	$\min_{\theta} max\{H(P_M), c\}$, where $c < \log k$

Figure 4. Examples of continuous relaxations: $e_{i,j}, P_i, Q_i, P_M$, and H, represent indicator variables denoting if a given input image contains a given digit, the discrete distribution over digits 1 to 4, the discrete distribution over digits 5 to 8, the discrete distribution over values 1 to M, and the entropy function, respectively.

a way of encoding the possible two digits in the cell indicated by data point x_i (one from $\{1...4\}$ and the other from $\{5...8\}$), is to use 8 binary variables $e_{i,j} \in \{0,1\}$, while requiring $\sum_{j=1}^{4} e_{i,j} = 1$ and $\sum_{j=5}^{8} e_{i,j} = 1$. In DRNets, we model probability distribution P_i and Q_i over digits 1 to 4 and 5 to 8 respectively: $P_{i,j,j=1...4}$ and $Q_{i,j,j=1...4}$ denote the probability of digit j and the probability of digit $j+4$, respectively. We approximate the cardinality constraint of $e_{i,j}$ by minimizing the entropy of P_i and Q_i, which encourages P_i and Q_i to collapse to one value. Another combinatorial constraint in Multi-MNIST-Sudoku is the All-Different constraint, where all the cells in a *constrained set* S, i.e., each row, column, and any of four 2x2 boxes involving the corner cells, must be filled with non-repeating digits. For a probabilistic relaxation of the All-Different constraint, we analogously define the entropy of the averaged digit distribution for all cells in a constrained set S, i.e., $H(\bar{P}_S)$:

$$H(\bar{P}_S) = -\sum_{j=1}^{4} \left(\frac{1}{|S|} \sum_{i \in S} P_{i,j} \right) \log \left(\frac{1}{|S|} \sum_{i \in S} P_{i,j} \right)$$

In this equation, a larger value implies that the digits in the cells of S distribute more uniformly. Thus, we can analogously approximate All-Different constraints by maximizing $H(\bar{P}_S)$ and $H(\bar{Q}_S)$. One can see, by minimizing all $H(P_i)$ and $H(Q_i)$ to 0 as well as maximizing all $H(\bar{P}_S)$ and $H(\bar{Q}_S)$ to $\log |S|$, we find a valid solution for the two 4x4 Sudoku puzzles, where all $P_{i,j}$ are either 0 or 1. We also relax k-sparsity constraints, which for example in Crystal-Phase-Mapping state the maximum number k of pure phases in an XRD-pattern, by minimizing the entropy of the phase distribution P_M below a threshold $c < \log k$. We choose the threshold $c < \log k$ because the entropy of a discrete distribution P_M concentrated on at most k values cannot exceed $\log k$. Note that other relaxations can be adapted in DRNets, for these and other tasks.

Constraint-Aware Stochastic Gradient Descent: We introduce a variant of standard SGD method called constraint-aware SGD, which is conceptually similar to the optimization process in GraphRNN (You et al., 2018), to tackle the optimization of global penalty functions $\psi_j^g(\{\phi_\theta(\mathbf{x}_k)|k \in S_j\})$, which involve several (potentially all) data points. We define a *constraint graph*, an undirected graph in which each data point forms a vertex and two data points are linked if they are in the same global constraint. Constraint-aware SGD batches data points from the randomly sampled (maximal) connected components in the *constraint graph*, and optimizes the objective function w.r.t. the subset of global constraints concerning those data points and the associated local constraints. For example, in Multi-MNIST-Sudoku, each overlapping Sudoku forms a maximal connected component, we batch the data points from several randomly sampled overlapping Sudokus and optimize the All-Different constraints (global) as well as the cardinality constraints (local) within them. However, in Crystal-Structure-Phase-Mapping, the maximal connected component becomes too large to batch together, due to the constraints (*phase field connectivity* and *Gibbs-alloying rule*) concerning all data points in the composition graph. Thus, we instead only batch a subset (still a connected component) of the maximal connected component – e.g., a path in the constraint graph, and optimize the objective function that only concerns constraints within the subset (along the path). By iteratively solving sampled local structures of the "large" maximal component, we cost-efficiently approximate the entire global constraint. Moreover, for optimizing the overall objective, constraint-aware SGD dynamically adjusts the

Algorithm 1 Constraint-aware stochastic gradient descent optimization of deep reasoning networks.

Input: **(i)** Data points $\{x_i\}_{i=1}^{N}$. **(ii)** Constraint graph. **(iii)** Penalty functions $\psi^l(\cdot)$ and $\psi_j^g(\cdot)$ for the local and the global constraints. **(iv)** Pre-trained or parametric generative decoder $G(\cdot)$.

1: Initialize the penalty weights λ^l, λ_j^g and thresholds for all constraints.
2: **for** number of optimization iterations **do**
3: Batch data points $\{\mathbf{x}_1, ..., \mathbf{x}_m\}$ from the randomly sampled (maximal) connected components.
4: Collect the global penalty functions $\{\psi_j^g(\cdot)\}_{j=1}^{M}$ concerning those data points.
5: Compute the latent space $\{\phi_\theta(\mathbf{x}_1), ..., \phi_\theta(\mathbf{x}_m)\}$ from the encoder.
6: Adjust the penalty weights λ_l, λ_j^g and thresholds accordingly.
7: minimize $\frac{1}{m} \sum_{i=1}^{m} \mathcal{L}(G(\phi_\theta(\mathbf{x}_i)), \mathbf{x}_i) + \lambda_l \psi^l(\phi_\theta(\mathbf{x}_i)) + \sum_{j=1}^{M} \lambda_j^g \psi_j^g(\{\phi_\theta(\mathbf{x}_k)|k \in S_j\})$ using any standard gradient-based optimization method and update the parameters θ.
8: **end for**

thresholds and the weights of constraints according to their satisfiability, which can involve non-differentiable functions. For efficiency and robustness, DRNets solve all instances together using constraint-aware SGD (see Algorithm 1).

4. Experiments

We illustrate the power of DRNets on two pattern de-mixing tasks – disentangling two overlapping hand-written Sudokus (**Multi-MNIST-Sudoku**) and inferring crystal structures of materials from X-ray diffraction data (**Crystal-Structure-Phase-Mapping**). Note that, since DRNets are an unsupervised framework, we can apply the *restart* (Gomes et al., 1998) mechanism, i.e., we can re-run DRNets for instances that do not satisfy all constraints. All the experiments are performed on one NVIDIA Tesla V100 GPU with 16GB memory. For the training process of our DRNets, we select a learning rate in $\{0.0001, 0.0005, 0.001\}$ with Adam optimizer (Kingma & Ba, 2014), for all the experiments. For baseline models, we followed their original configurations and further fine-tuned their hyper-parameters to saturate their performance on our tasks.

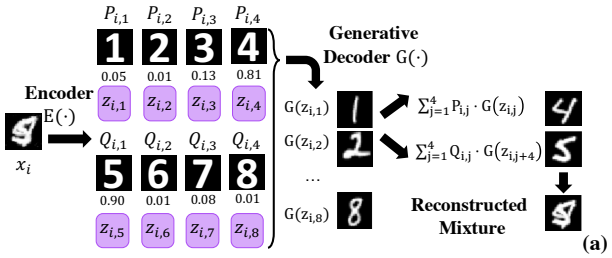

Method	Training Set Size	Test Set Size	Accuracy (%)		Time
			Sudoku	Digit	
DRNets	N/A	16×10,000 overlapping digits	**98.6**	**99.9**	28min
DRNets w/ Restart			**100.0**	**100.0**	50min
DRNets w/o Reasoning			15.0	88.8	110min
CapsuleNet	16×10,000 overlapping digits		50.9	97.9	1min+30min
CapsuleNet + local search			57.8	97.9	3hours+30mins
ResNet-18			68.5	97.7	3min+10hours
ResNet-18 + local search			88.3	97.7	3hours+10hours

(b)

Figure 5. **(a)** The latent space of DRNets for Multi-MNIST-Sudoku. **(b)** Accuracy comparison. We show "test time + training time" for supervised baselines, and "solving time" for DRNets.

4.1 Multi-MNIST-Sudoku: We generated 160,000 input data points for each training set, validation set and test set, where each data point corresponds to a 32x32 image of overlapping digits coming from MNIST (LeCun et al., 1998) and every 16 data points form a 4-by-4 overlapping Sudokus. The training set and the validation set are only used by supervised baselines while DRNets directly solve the test set without using them. For DRNets, we also generated an extra *cGan* dataset, which is composed of 25,000 *original MNIST images* for pre-training the conditional GAN. Note that these four datasets are generated using disjoint sets of MNIST images. For Multi-MNIST-Sudoku, the encoder of DRNets is composed of two ResNet-18 (He et al., 2016) networks and we use a conditional GAN (Mirza & Osindero, 2014) as our generative decoder (denoted as $G(\cdot)$), which is trained using the digits in the *cGan* dataset. Note that this is the only supervision we have in this task, which is even weaker than the general concept of the *weakly-supervised setting* (Zhang et al., 2017). DRNets batch every 16 data points together to enforce the All-Different constraints among the cells of each Sudoku. As shown in Fig.5a, given the input cell $\mathbf{x}_i$, two networks encode a two-part latent space: one encoder network has a 8-dimensional output layer and models the two distributions P_i and Q_i for the two overlapping digits; the other encoder network outputs eight 100-dimensional (800 dimensions in total) latent encoding $z_{i,j}$ to encode the shape of the possible eight digits conditioned on the input mixture, and is used by the generative decoder to generate the reconstructed digits $G(z_{i,j})$. DRNets estimate the two digits in the cell by computing the expected digits over P_i and Q_i, i.e., $\sum_{j=1}^{4} P_{i,j} G(z_{i,j})$ and $\sum_{j=1}^{4} Q_{i,j} G(z_{i,j+4})$, and reconstruct the original input mixture.

We used the L1-loss as the reconstruction loss with a weight of 0.001. The reasoning loss enforces the Sudoku rules and includes the continuous relaxation of the cardinality (2×16 cells) and All-Different (2×(4 rows + 4 columns + 4 boxes)) constraints for every 16 data points, with initial weights of 0.01 and 1.0, respectively.

To demonstrate the power of reasoning, we compared our unsupervised DRNets with supervised start-of-the-art MNIST de-mixing models – CapsuleNet (Sabour et al., 2017) and ResNet (He et al., 2016), and a variant of DRNets that removes the reasoning modules ("DRNets w/o Reasoning"). To saturate the performance of baseline models, we also applied a post-process local search for them to incorporate the Sudoku Rules. Specifically, we did a local search for the top-2 (top-3 would take too long to search) most likely choice of digits for each Sudoku of the two overlapping Sudokus and try to satisfy Sudoku rules with minimal modification compared with the original prediction. We evaluate both the percentage of digits that are correctly de-mixed (digit accuracy) and the percentage of overlapping Sudokus that have all digits correctly de-mixed (Sudoku accuracy). Empowered by reasoning, DRNets significantly outperformed CapsuleNet, ResNet, and DRNets without reasoning, perfectly recovered all digits with the *restart* mechanism (see Fig.5b), and additionally reconstructed the mixed images with high-quality (see Fig.1).

4.2 Crystal-Structure-Phase-Mapping concerns inferring crystal structures from a set of X-ray diffraction measurements (XRDs) of a given chemical system, satisfying thermodynamic rules. Crystal structure phase mapping is a very challenging task, a major bottleneck in high-throughput ma-

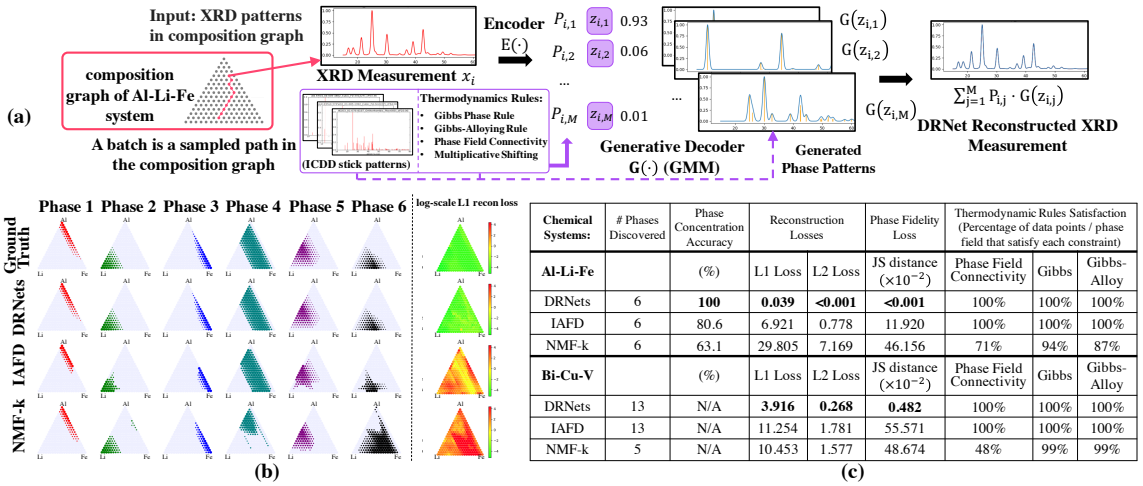

Chemical Systems:	# Phases Discovered	Phase Concentration Accuracy	Reconstruction Losses		Phase Fidelity Loss	Thermodynamic Rules Satisfaction (Percentage of data points / phase field that satisfy each constraint)		
Al-Li-Fe		(%)	L1 Loss	L2 Loss	JS distance ($\times 10^{-2}$)	Phase Field Connectivity	Gibbs	Gibbs-Alloy
DRNets	6	**100**	**0.039**	**<0.001**	**<0.001**	100%	100%	100%
IAFD	6	80.6	6.921	0.778	11.920	100%	100%	100%
NMF-k	6	63.1	29.805	7.169	46.156	71%	94%	87%
Bi-Cu-V		(%)	L1 Loss	L2 Loss	JS distance ($\times 10^{-2}$)	Phase Field Connectivity	Gibbs	Gibbs-Alloy
DRNets	13	N/A	**3.916**	**0.268**	**0.482**	100%	100%	100%
IAFD	13	N/A	11.254	1.781	55.571	100%	100%	100%
NMF-k	5	N/A	10.453	1.577	48.674	48%	99%	99%

Figure 6. **(a)** The latent space of DRNets for Crystal-Structure-Phase-Mapping. M denotes the number of possible phases. (For Al-Li-Fe, $M = 159$; For Bi-Cu-V, $M = 100$.) **(b)** Comparison of phase concentration and reconstruction loss for different methods in Al-Li-Fe oxide system. Note that, 6 pure phases (out of 159 possible candidates) appear in the system and result in 15 different types of mixtures. Each dot represents an XRD measurement whose size is proportional to the estimated phase concentration. DRNet's phase concentration closely match the ground truth in contrast to IAFD's and NMF-k's. The heatmap on the right shows that DRNets reconstruct the XRD measurements much better than other methods with respect to the L1 loss. **(c)** DRNets outperform both IAFD and NMF-k with all evaluation criteria on both systems.

terials discovery: Each X-ray measurement may involve several mixed crystal structures; each chemical system includes hundreds of possible crystal structures; for each crystal structure pattern, we only have an *idealized* model of pure crystal phases; the thermodynamic rules are also complex; the crystal patterns are difficult for human experts to interpret; and we only have hundreds of (unlabeled) data points for each chemical system, which greatly challenges classical data-hungry deep learning models.

Herein, we illustrate DRNets for crystal structure phase mapping for two chemical systems: (1) a ternary **Al-Li-Fe** oxide system (Le Bras et al., 2014), which is theoretically based, synthetically generated, with ground truth solutions, and (2) a ternary **Bi-Cu-V** oxide system, which is a more challenging real experiment-based system, more noisy and uncertain. For each system, the input data points are mixtures of XRDs, associated with a *composition graph* identifying elemental compositions and the *constraint graph* of data points, in which there is an edge between two data points if they share a constraint. Specifically, each data point is associated with a D-dimensional vector representing the intensity of the mixture of XRDs at different diffraction angles (referred as Q values) and a 3-dimensional composition vector representing the proportion of the three different metal elements at that data point (e.g., [80% of Al, 5% of Fe, 15% of Li]). Since there are only 2 degrees of freedom in the composition vector, we can map each data point into a 2-D triangular composition space (See Fig.6a) and build the *composition graph* by adding edges between the data points in the 2-D triangular composition space through Delaunay triangulation. We also collected a library of known crystal structures from the International Centre for Diffraction Data (ICDD) database. Each crystal structure (also named *phase*) is given as a list of diffraction peak location-amplitude pairs, (referred to as *stick pattern*), representing the ideal phase patterns measured in perfect conditions (see Fig.6a). For the Al-Li-Fe oxide system, we have 231 data points (mixtures of XRDs) in the composition space, 159 known stick patterns for the known phases, and each data point has 650 different Q values $Q_i \in [15°, 80°]$ and the corresponding intensities $I_i \in [0, 1]$. For the Bi-Cu-V oxide system, we have 307 data points in the composition space, 100 ICDD known stick patterns, and each data point has 4096 different Q values $Q_i \in [5°, 45°]$ and the corresponding intensities $I_i \in [0, 1]$. To better use the memory, we down-sampled the raw data of Bi-Cu-V oxide system to 300 different Q values.

Given the input D-dimensional vector representing the intensity of the mixture of XRDs at different diffraction angles, we use four 3-layer-fully-connected networks as our encoder to encode a two-part latent space, which captures the probabilities (denoted as $P_{i,j}$) and shapes of the possible phases (denoted as $z_{i,j}$) and is constrained by the reasoning module to satisfy the thermodynamic rules (See Fig.6a). To model more realistic conditions, the generative decoder of the DRNets use Gaussian mixture models (Lindsay, 1995) to approximate the real phase patterns from *stick patterns* where the relative peak locations and mixture coefficients are given by the stick locations and amplitudes and the

peak width, multiplicative location shift, and possible amplitude variance are parameterized by the latent encoding $z_{i,j}$. The overall objective function of the DRNets combines responses from the generative decoder and the reasoning module, which is optimized using constraint-aware stochastic gradient descent. Specifically, the output of the first three networks in the encoder are M-dimensional vectors: $(P_{i,1}, ..., P_{i,M})$, $(\alpha_{i,1}, ..., \alpha_{i,M})$, $(\sigma_{i,1}, ..., \sigma_{i,M})$ (M is the number of possible phases, e.g., 159 for the Al-Fe-Li oxide system), which represent the probability $P_{i,j}$ of each phase-j at data point i, the multiplicative shifting ratio $\alpha_{i,j}$, and the standard deviation $\sigma_{i,j}$ of the Gaussians characterizing the peaks in phase-j, respectively. The output of the last network is a $M \times K$-dimensional vector, representing the possible amplitude variance of peaks in each phase. Here, K is the number of maximal peaks in a stick pattern ($K = 200$). For the first 3 networks there are 1024, 1024, and 512 hidden units, respectively per layer, and for the last network there are 512, 512, and 32 hidden units, respectively per layer. The last layer has fewer hidden units given its high-dimensional output space ($M \times K$). All networks use ReLU (Nair & Hinton, 2010) as their activation function.

In crystal-structure-phase-mapping, we impose the following thermodynamic rules: *Phase Field Connectivity*, *Gibbs Phase Rule* and *Gibbs-Alloying Rule* (Gomes et al., 2019). As stated in the section 3, we solve the large global constraints (e.g., *Phase Field Connectivity*) via sampling their local structure and solving each of them iteratively. Specifically, for each oxide system, we sampled 100,000 paths in the composition graph via Breadth First Search to construct a path pool. Then, for every iteration, DRNets randomly sample a path from the pool and batch the data points along that path (see Fig. 6). Finally, we only reason about the thermodynamic rules along the path and solve the global constraints iteratively . In this task, we used the Jensen-Shannon distance (JS distance) with a weight of 20.0 plus the L2-distance with a weight of 0.05 as the reconstruction loss. We use the JS distance since the location of peaks are the most important characteristics of a phase pattern and mismatching peaks would cause a large JS distance. To compute the JS distance, we normalize the area under each XRD pattern to be 1 and use a ϵ of 1e-9 to avoid division by zero. Due to the different noise level, we use different weights for *Gibbs Rule* (1.0 and 30.0) and *Phase Field Connectivity* (0.01 and 3.0) for Al-Li-Fe oxide system and Bi-Cu-V oxide system respectively.

We compared DRNets with IAFD (Gomes et al., 2019) and NMF-k (Stanev et al., 2018), which are both state-of-the-art non-negative matrix factorization (NMF) based unsupervised de-mixing models for crystal-structure-phase-mapping. NMF-k improves the pure NMF algorithm (Long et al., 2009) by clustering common phase patterns from thousands of runs. However, NMF-k does not directly enforce thermodynamic rules and therefore the solutions produced are often not completely physically meaningful. IAFD uses external mixed-integer programming modules to enforce thermodynamic rules during the de-mixing. However, due to the gap between the external optimizer and NMF module, the solution of IAFD satisfies constraints at the cost of huge reconstruction loss and is still far from the ground truth. Our evaluation criteria include phase concentration accuracy (i.e., accuracy of the combination of de-mixed phases for each XRD mixture, only available for Al-Li-Fe system), phase fidelity loss, reconstruction losses, and the satisfaction of thermodynamic rules. Note that, before evaluating the reconstruction losses, we fit the de-mixed phases (for all methods) to the closest idealized phases using the stick patterns to exclude noise (Le Bras et al., 2014). Meanwhile, we quantified the phase fidelity loss by measuring the JS distance between the de-mixed phases and the closest ideal phases. Note that, only DRNets and NMF-k can determine the number of discovered phases automatically. Thus, we provide extra information (ground-truth/experts' conclusion) for IAFD to set $k = 6$ ($k = 13$) for Al-Li-Fe (Bi-Cu-V) oxide system. As shown in the Fig.6b-c, for the Al-Li-Fe oxide system, the phase concentration (the distribution of de-mixed pure phases over all data points of that chemical system) of either IAFD or NMF-k is far from the ground truth. In contrast, DRNet almost exactly recovered the ground truth solution (100% concentration accuracy) by seamlessly integrating pattern recognition, reasoning and prior knowledge. Moreover, by explicitly incorporating the ICDD stick pattern information into DRNets, the phases de-mixed by DRNets are much closer to the ICDD patterns than those from IAFD and NMF-k (see phase fidelity loss). For Bi-Cu-V oxide system, DRNets solved this *previously unsolved* real system, producing valid crystal structures and significantly outperforming IAFD and NMF-k w.r.t. reconstruction errors and phase fidelity loss. In addition, materials science experts thoroughly checked DRNet's solution of Bi-Cu-V oxide system, approved it, and subsequently discovered a new material that is important for solar fuels technology. In contrast, neither the solution from NMF-k nor IAFD is completely physically meaningful.

5. Conclusions and future work

We propose DRNets, a powerful end-to-end framework that combines deep learning with constraint reasoning for solving unsupervised pattern de-mixing tasks. DRNets outperform the state of the art for de-mixing MNIST Sudokus and crystal-structure phase mapping, solving previously unsolved chemical systems and leading to the discovery of new solar fuels materials, substantially beyond the reach of other methods and materials science experts' capabilities. Future research includes exploring DRNets for incorporating other types of constraints, prior knowledge, objective functions,

and even label supervision for other applications.

Acknowledgements

This research was supported by NSF awards CCF-1522054 (Expeditions in computing) and CNS-1059284 (Infrastructure), AFOSR Multidisciplinary University Research Initiatives (MURI) Program FA9550-18-1-0136, ARO awards W911NF-14-1-0498 and W911NF-17-1-0187, US DOE Award No. DE-SC0020383, and an award from the Toyota Research Institute. Materials science experiments were supported by US DOE Award No. DE-SC0004993. Use of SSRL is supported by DOE Contract No. DE-AC02-76SF00515. We are grateful for the assistance of Junwen Bai for running the IAFD baseline and Aniketa Shinde for photoelectrochemistry experiments.

References

Bai, J., Bjorck, J., Xue, Y., Suram, S. K., Gregoire, J., and Gomes, C. Relaxation methods for constrained matrix factorization problems: solving the phase mapping problem in materials discovery. In *International Conference on AI and OR Techniques in Constraint Programming for Combinatorial Optimization Problems*, pp. 104–112. Springer, 2017.

Bai, J., Ament, S., Perez, G., Gregoire, J., and Gomes, C. An efficient relaxed projection method for constrained non-negative matrix factorization with application to the phase-mapping problem in materials science. In *International Conference on the Integration of Constraint Programming, Artificial Intelligence, and Operations Research*, pp. 52–62. Springer, 2018.

Ermon, S., Le Bras, R., Suram, S. K., Gregoire, J. M., Gomes, C. P., Selman, B., and Van Dover, R. B. Pattern decomposition with complex combinatorial constraints: Application to materials discovery. In *Twenty-Ninth AAAI Conference on Artificial Intelligence*, 2015.

Ganchev, K., Gillenwater, J., Taskar, B., et al. Posterior regularization for structured latent variable models. *Journal of Machine Learning Research*, 11(Jul):2001–2049, 2010.

Garcez, A. d., Gori, M., Lamb, L. C., Serafini, L., Spranger, M., and Tran, S. N. Neural-symbolic computing: An effective methodology for principled integration of machine learning and reasoning. *arXiv preprint arXiv:1905.06088*, 2019.

Gomes, C. P., Selman, B., Kautz, H., et al. Boosting combinatorial search through randomization. *AAAI/IAAI*, 98: 431–437, 1998.

Gomes, C. P., Bai, J., Xue, Y., Björck, J., Rappazzo, B., Ament, S., Bernstein, R., Kong, S., Suram, S. K., van Dover, R. B., et al. Crystal: a multi-agent ai system for automated mapping of materials' crystal structures. *MRS Communications*, pp. 1–9, 2019.

He, K., Zhang, X., Ren, S., and Sun, J. Deep residual learning for image recognition. In *Proceedings of the IEEE conference on computer vision and pattern recognition*, pp. 770–778, 2016.

Hinton, G. E., Ghahramani, Z., and Teh, Y. W. Learning to parse images. In *Advances in neural information processing systems*, pp. 463–469, 2000.

Hu, Z., Ma, X., Liu, Z., Hovy, E., and Xing, E. Harnessing deep neural networks with logic rules. *arXiv preprint arXiv:1603.06318*, 2016a.

Hu, Z., Yang, Z., Salakhutdinov, R., and Xing, E. Deep neural networks with massive learned knowledge. In *Proceedings of the 2016 Conference on Empirical Methods in Natural Language Processing*, pp. 1670–1679, 2016b.

Kingma, D. and Ba, J. Adam: A method for stochastic optimization. *arXiv preprint arXiv:1412.6980*, 2014.

Le Bras, R., Bernstein, R., Gregoire, J. M., Suram, S. K., Gomes, C. P., Selman, B., and Van Dover, R. B. Challenges in materials discovery–synthetic generator and real datasets. In *Twenty-Eighth AAAI Conference on Artificial Intelligence*, 2014.

LeCun, Y., Bottou, L., Bengio, Y., Haffner, P., et al. Gradient-based learning applied to document recognition. *Proceedings of the IEEE*, 86(11):2278–2324, 1998.

Lindsay, B. G. Mixture models: theory, geometry and applications. In *NSF-CBMS regional conference series in probability and statistics*, pp. i–163. JSTOR, 1995.

Long, C., Bunker, D., Li, X., Karen, V., and Takeuchi, I. Rapid identification of structural phases in combinatorial thin-film libraries using x-ray diffraction and non-negative matrix factorization. *Review of Scientific Instruments*, 80(10):103902, 2009.

Manhaeve, R., Dumancic, S., Kimmig, A., Demeester, T., and De Raedt, L. Deepproblog: Neural probabilistic logic programming. In *Advances in Neural Information Processing Systems*, pp. 3749–3759, 2018.

Mirza, M. and Osindero, S. Conditional generative adversarial nets. *arXiv preprint arXiv:1411.1784*, 2014.

Nair, V. and Hinton, G. E. Rectified linear units improve restricted boltzmann machines. In *Proceedings of the 27th international conference on machine learning (ICML-10)*, pp. 807–814, 2010.

Pathak, D., Krahenbuhl, P., and Darrell, T. Constrained convolutional neural networks for weakly supervised segmentation. In *Proceedings of the IEEE international conference on computer vision*, pp. 1796–1804, 2015.

Robbins, H. and Monro, S. A stochastic approximation method. In *Herbert Robbins Selected Papers*, pp. 102–109. Springer, 1985.

Sabour, S., Frosst, N., and Hinton, G. E. Dynamic routing between capsules. In *Advances in neural information processing systems*, pp. 3856–3866, 2017.

Shivhare, R. and Kumar, C. A. On the cognitive process of abstraction. *Procedia Computer Science*, 89:243–252, 2016.

Stanev, V., Vesselinov, V. V., Kusne, A. G., Antoszewski, G., Takeuchi, I., and Alexandrov, B. S. Unsupervised phase mapping of x-ray diffraction data by nonnegative matrix factorization integrated with custom clustering. *npj Computational Materials*, 4(1):43, 2018.

Wang, P.-W., Donti, P. L., Wilder, B., and Kolter, Z. Satnet: Bridging deep learning and logical reasoning using a differentiable satisfiability solver. *arXiv preprint arXiv:1905.12149*, 2019.

Xu, J., Zhang, Z., Friedman, T., Liang, Y., and Broeck, G. V. d. A semantic loss function for deep learning with symbolic knowledge. *arXiv preprint arXiv:1711.11157*, 2017.

Xue, Y., Bai, J., Le Bras, R., Rappazzo, B., Bernstein, R., Bjorck, J., Longpre, L., Suram, S. K., van Dover, R. B., Gregoire, J., et al. Phase-mapper: an ai platform to accelerate high throughput materials discovery. In *Twenty-Ninth IAAI Conference*, 2017.

You, J., Ying, R., Ren, X., Hamilton, W. L., and Leskovec, J. Graphrnn: Generating realistic graphs with deep auto-regressive models. *arXiv preprint arXiv:1802.08773*, 2018.

Zhang, N., Yan, J., and Zhou, Y. Weakly supervised audio source separation via spectrum energy preserved wasserstein learning. *arXiv preprint arXiv:1711.04121*, 2017.

Zhou, X., Sun, X., Zhang, W., Liang, S., and Wei, Y. Deep kinematic pose regression. In *European Conference on Computer Vision*, pp. 186–201. Springer, 2016.

Zhou, X., Huang, Q., Sun, X., Xue, X., and Wei, Y. Weakly-supervised transfer for 3d human pose estimation in the wild. In *IEEE International Conference on Computer Vision*, volume 206, pp. 3, 2017.